THE UNIVERSITY of EDINBURGH

Edinburgh Research Explorer

Shear strengthening masonry panels with sheet glass-fiber reinforced polymer

OPEN ACCESS

Shear strengthening masonry panels with sheet GFRP

Manuscript number CC-22306

Tim Stratford [1], Giovanni Pascale [2], Odine Manfroni [3] and Barbara Bonfiglioli [4]

1   *Lecturer.   Institute of Infrastructure and Environment, The University of Edinburgh, The King's Buildings, Edinburgh, EH9 3JN, UK*

2   Associate Professor.   DISTART, Dept. of Structural Engineering, University of Bologna, Viale Risorgimento 2, I-40136 Bologna, Italy.

3   Consultant Civil Engineer. Manfroni Engineering Workshop (MEW), v. G. Pascoli, 39 - Santarcangelo di Romagna, I-47822, Rimini, Italy.

4   Research Fellow.   DISTART, Dept. of Structural Engineering. University of Bologna, Viale Risorgimento 2, I-40136 Bologna, Italy.

ABSTRACT

This paper investigates strengthening masonry walls using glass-fiber reinforced polymer (GFRP) sheets.

An experimental research program was undertaken. Both clay and concrete brick specimens were tested, with and without GFRP strengthening. Single-sided strengthening were considered, as it is often not practicable to apply the reinforcement to both sides of a wall. Static tests were carried out on six masonry panels, under a combination of vertical pre-load, and in-plane horizontal shear loading. The mechanisms by which load was carried were observed, varying from the initial, uncracked state, to the final, fully cracked state.

The results demonstrate that a significant increase of the in-plane shear-capacity of masonry can be achieved by bonding GFRP sheets to the surface of masonry walls. The experimental data were used to assess the effectiveness of the GFRP strengthening, and suggestions are made to allow the test results to be used in the design of sheet GFRP strengthening for masonry structures.

INTRODUCTION

One of the many structural applications of fiber-reinforced-polymer (FRP) materials is for strengthening masonry buildings. Masonry strengthening is of particular interest in countries prone to seismic activity, but is also of benefit where masonry structures require repair, or a change in use requires structural upgrade.

The benefits of FRP strengthening systems have been discussed elsewhere, for example in Triantafillou (1998), Arduini and Nanni (1997), Fam et al. (1997), but it is worth briefly reviewing them here:-

- good corrosion resistance

- ease of application to an existing structure

- adaptability of the strengthening solution to a particular application

- unobtrusive repair, particularly important for historic structures

- high strength-to-mass and stiffness-to-mass ratios, which are of particular importance for seismic strengthening since they do not significantly increase the dynamic mass of the structure

  However, it is also important to note possible disadvantages of FRP strengthening:

- the binding resins presently used are flammable, and give off toxic vapors during a fire (Kolsch,1998)

- the long-term reliability of the materials is largely unproven

- FRPs are impermeable to moisture transport

A variety of approaches has previously been investigated for strengthening masonry using FRP. For high-value, historically important buildings (often including domes, spires or vaults), non-intrusive, localized reinforcement schemes can often be devised.

However, non-historic, "utility" structures may also require strengthening. In these buildings, aesthetics typically do not govern and the reinforcement can be applied to a larger area of the structure. A simple strengthening system is required, which is easily applied to any general structure.

One approach to strengthening is to embed FRP rods into the horizontal joints of a masonry wall (Fig. 1a) (Tinazzi et al. 2000, Tumialan et al. 2001). Amongst the advantages of this method is the lack of visible alteration to the structure and the minimization of binding resins, however, inserting the FRP rods and re-pointing the masonry is labor-intensive.

An alternative approach is to apply the FRP over the surface of the masonry. Strips of FRP, containing unidirectional fibers, can be bonded to the surface of a wall, and arranged to give an external truss system, tailored according to the applied load (Fig. 1b). This truss strengthening system has been studied by Schwegler (1994).

The present work considers sheet FRP, adhesively bonded to the whole surface of the masonry (Fig. 1c). The advantage of this approach to strengthening is its simplicity. Previous research into this subject includes work by Ehsani (1995) and Al-Saidy et al. (1996) to repair a single-story, earthquake damaged building in California. Hamid et al. (1993) carried out shear tests on small, hollow concrete block specimens and further tests were undertaken by Schwegler (1994). Dynamic tests have been conducted by Marshall et al. (1999), while Luciano & Sacco (1998) have studied finite element modeling of FRP-reinforced masonry.

This paper describes an experimental investigation of in-plane shear strengthening using sheet glass-fiber-reinforced-polymer (GFRP). Only one side of the masonry was strengthened, since single-sided strengthening could be more economic and allows the façade of a building to be left untouched.

EXPERIMENTAL PROGRAM

The construction of the GFRP-strengthened masonry specimens tested during this study is shown in Fig. 2.

Specimen construction

The test specimens were based upon a 1.2 m square, stretcher-bond, brick-masonry panel. Six masonry panels were constructed, three from clay bricks and three from concrete bricks. New bricks were used throughout, with the same mortar used for all specimens. One specimen of each material was left unreinforced, while the other two were strengthened using GFRP. The different specimens are listed in Table 1.

A sheet GFRP with a biaxial weave was applied to the masonry. The GFRP had equal amounts of fiber in the horizontal and vertical directions (parallel to the mortar joints). GFRP in which the fibers are oriented at 45° to the joints is more intuitive for shear strengthening, but is less easily applied. The GFRP was applied using a wet lay-up procedure:

- The panels were thoroughly cleaned using a combination of abrasion and a solvent before any polymer products were applied.

- A filler layer was applied to give a flat surface. A cement render was used on the concrete walls, and an epoxy filler was applied to the clay specimens.

- An epoxy primer was used to seal pores in the masonry, so that subsequent applications of epoxy were not absorbed by the wall (the primer coat was applied directly to the clay bricks, and over the render on the concrete specimens).

- Epoxy adhesive was used to bond the GFRP to the panel, with a final coat of adhesive to ensure

saturation of the fibers.

- The GFRP was cut longer than the wall's height and wrapped around the top and bottom of the masonry panel. This GFRP was trapped by the test rig, providing anchorage of the GFRP along the top and bottom edges of the specimen.

Test arrangement

Figs. 3 & 4 show the testing arrangement. A combination of vertical compression (representing loads from the building above) and in-plane shear load was applied to each specimen.

The vertical prestress load was applied through two connected hydraulic jacks (N). This load was distributed across the top of the specimen by a stiff steel reaction beam, which was restrained horizontally by steel bars. The load was transferred across a flat polytetrafluoroethylene (PTFE) bearing, into a steel cap beam on top of the wall. The bearing allowed the cap beam to slide horizontally relative to the reaction beam.

The shear load was applied to the wall by a horizontal hydraulic jack (P). To assess the proportion of this load carried across the PTFE bearing by friction, strain gauges were attached to the steel bars, giving the horizontal reaction force (H).

The horizontal deflection was measured using a displacement transducer at the same level as the load application point, on the opposite side of the wall (δ). Strain gauges were applied to the surface of the GFRP, to measure the strain along the tensile diagonal.

The possibility of the specimen twisting (as the GFRP was applied to only one side of the panel) had been considered prior to testing and restraint against twisting was provided in the testing arrangement. The slack in this restraint was not taken up during testing, suggesting that there was negligible twisting.

Loading sequence

A vertical prestress of N=100 kN was first applied to the wall. The horizontal load (P) was then increased in increments of 10 kN. Once 50 kN was reached, and after each subsequent loading increment, P was reduced to 40 kN to allow the specimen to be inspected.

Due to the limitations of the available equipment, it was not possible to maintain a constant vertical prestress during the tests. The wall tended to rotate as the horizontal load was applied, so that the vertical load increased with the applied horizontal load.

EXPERIMENTAL RESULTS

Characterization of materials

Table 2 gives the results of the various materials tests carried out to support the experimental program, with the test method by which they were obtained.

In addition, pull-off tests were conducted to characterize the interface between the masonry and the GFRP. The de-bonded surfaces of a clay and a concrete pull-off specimen are shown in Figs. 5a and 5b. There was good adhesion between the clay and the GFRP, with de-bonding occurring at the brick-adhesive interface or between the epoxy filler and adhesive layers at an average pull-off strength of 3.87 MPa. In the concrete specimen, failure was in the mortar rendering, with an average pull-off strength of only 0.59 MPa.

Failure of the masonry

Figs. 6 to 9 record the crack pattern in the exposed masonry face for one of each type of specimen tested. In all cases, except for the unreinforced clay specimen, the masonry panels failed by rapid propagation of a diagonal crack, which followed the mortar joints. The unreinforced clay wall failed along a near-horizontal crack at the base of the wall, dominated by sliding along the mortar-brick interface. This was due to the use of smooth clay bricks without any type of surface indentation.

Tensile and shear modes of joint failure mostly occurred at the brick-mortar interface rather than in the mortar itself, particularly in the smooth-surfaced clay bricks (this is apparent in Figs. 6 & 8). In a few places (for example, the top-left of Fig. 7), a tensile crack jumped across a brick, between two header joints. Compressive failure was by crushing of the mortar, as the compressive strength of the bricks was much higher than that of the mortar.

In the walls strengthened with GFRP, a slightly more distributed band of cracking formed.

Failure of the GFRP strengthening

Failure of the strengthening did not occur in the GFRP itself, but by de-bonding of the GFRP from the surface of the panel. Fig. 10 shows the extent of de-bonding for a strengthened clay panel, mapped by tapping the surface of the wall and noting where it sounded hollow.

Small regions of local de-bonding initially formed near the load application point (at 150 kN), and the reaction point (at 190 kN). At the ultimate load (195 kN) the de-bonded region spread suddenly, roughly along the compressive diagonal.

De-bonding of the GFRP from the masonry occurred in the same manner as in the small-scale pull-off specimens. In the clay walls, failure was either at the epoxy-brick interface (possibly due to imperfect cleaning), between the adhesive and filler layers, or beneath the surface of the brick (Fig. 11). In the concrete walls, the failure was between the cement render and the bricks.

Load-deflection responses

The load-deflection responses of the clay and concrete specimens are plotted in Fig. 12. The shear load carried through the wall ($V=P-H$) is plotted against the horizontal deflection (δ). For clarity, only a single unload-reload loop has been shown in each figure.

Fig. 13 shows the load-strain response for sample concrete 2. The strain was measured towards the center of the wall, as shown in Fig. 4.

Strengthening the clay walls with GFRP increased the load-capacity from approximately 115 kN to 190 kN (an increase of 65%). For the concrete walls, the ultimate load increased from 80 kN to 110 kN for specimen 2 (a 38% increase), and 130 kN for specimen 3 (a 63% increase). The stiffness and deformation-capacity of the specimens was not changed by the GFRP.

The comparatively low failure load of the concrete walls was due to the lower mechanical properties of the concrete bricks and the use of an inappropriate mortar (as shown in Table 2). The concrete bricks were porous and the mortar dried before it had properly cured.

ANALYSIS AND DISCUSSION OF RESULTS

The tests confirm that the load-capacity of masonry panels subjected to in-plane shear can be greatly increased by applying sheet GFRP. The success of a strengthening system, however, should not be considered simply in terms of an increase in failure load. The mechanisms by which both the masonry and the GFRP carry load should also be examined.

Unreinforced Masonry

The load-deflection plots for the unreinforced masonry panels in Fig. 12 are typical for masonry loaded in shear (Barsotti & Ligarò, 1998). The masonry is initially uncracked and has a linear-elastic response. Progressive cracking follows, giving a second phase with a reduced stiffness. Finally, there is a frictional plateau.

The behavior of the masonry was dominated by joint failure. As described above, two modes of joint failure were observed:

- Shear failure, involving sliding along a slip plane either within the mortar or at the brick-mortar interface.

- Crushing failure, which occurred when the compressive strength of the mortar was reached.

Interaction diagrams can be plotted showing these two limiting states and thus the domain of horizontal and vertical loads that can be carried by the masonry. Fig. 14 shows a typical interaction diagram, in which the non-dimensional vertical load, $n = N/(\overline{\sigma} b t_M)$, is plotted against the horizontal load, $v = V/(\overline{\sigma} b t_M)$. $\overline{\sigma}$ is the compressive strength of the masonry, b is the breadth of the masonry specimen, and t_M is its thickness. The vertical load at which the mode of failure changes from slipping to crushing is dependent upon the ratio $\eta = h/b$. where h and b are the height and breadth of the panel.

The work of Barsotti & Ligarò (1998) was used to construct the interaction diagrams for the clay and concrete walls tested in the present work (Fig. 15). The points representing failure of the unreinforced masonry specimens lie on the shear (slipping) failure limit, as observed during the tests.

Strengthened masonry

The load carried through the strengthened masonry is also shown on the interaction diagrams in Fig. 15. However, before considering these points, the mechanisms by which the GFRP strengthening acts will be discussed.

Fig. 16 plots the increase in load due to the GFRP (the difference between the strengthened and unreinforced load-deflection curves in Fig. 12). The mechanism by which the strengthened walls carry load changes with increasing deflection, giving three distinct parts, which are most apparent for the clay specimens. At small deflections, the GFRP is *fully-bonded* to the uncracked masonry and does not significantly increase the load carried by the wall. In the second mechanism, cracks form in the masonry and the GFRP debonds locally, accompanied by an approximately linear increase in load. Finally, a horizontal plateau indicates that the masonry is completely separated by a crack. These three mechanisms are illustrated in Fig. 17.

Uncracked, fully-bonded strengthening mechanism

The GFRP is initially fully-bonded and acts compositely with the masonry (Fig 17). The strengthened stiffness is not significantly greater than for the unreinforced masonry, so that the GFRP does not initially increase the load carried by the specimen (Fig. 16).

At a deflection of 2-3 mm for the clay specimens or 1-2 mm for the concrete specimens, local cracks form in the masonry and the GFRP starts to separate or *de-bond* from the masonry. Cracking and de-bonding

initiates at the concentrations of interfacial shear stress near the loading point and the reaction point (as shown in Fig. 10). Note that de-bonding of the interface is *not* a peeling failure (which involves direct tensile stress) as there is no out-of-plane bending. It is a *shear* delamination failure.

Propagation of cracks

The load at which cracks first formed is most clearly shown by the load-strain plot in Fig. 13. The strain is a measure of local deformation, rather than the global deformation plotted in Fig. 12. These cracks propagate until the specimen is completely separated into two pieces.

The spread of cracks across the masonry is accompanied by local de-bonding of the GFRP from the masonry, so that a band of de-bonded GFRP forms along a band roughly parallel to the cracks. The GFRP restrains the growth of cracks in the masonry, and thus the load carried by the strengthened specimens continues to increase with deflection (Fig. 16).

Fully cracked mechanism

Once a single crack has formed across the masonry, the two parts of the specimen slide relative to each other (Fig. 17c). This is accompanied by spread of the de-bonded area of GFRP back from the crack.

The de-bonded GFRP can carry only tension, and during the tests it buckled in the direction of the compressive diagonal, apparent as diagonal banding in Fig. 19. A fully-cracked panel thus carries shear by a truss mechanism; diagonal tensile action through the GFRP is reacted by a vertical compression in the masonry (Fig.17c).

The spread of de-bonded GFRP must be compatible with the crack opening width. Compatibility of the GFRP and masonry across the crack can be split into two components, as shown in Fig. 18:

- stretching of the de-bonded GFRP

- slip of the bonded GFRP relative to the masonry

Slip of the bonded GFRP relative to the masonry is greatest adjacent to the de-bonded GFRP, and reduces to zero (fully-bonded) along the anchorage length. The anchorage length and the force required to drive separation of the GFRP from the masonry remains constant as the de-bonded GFRP spreads back from the crack, so long as the width of GFRP remain constant. This is most apparent for specimen Clay 2 in Fig. 16, for which there is a distinct plateau once the specimen is fully cracked. Clay 3 exhibits a more gradual transition between the partially-cracked and fully-cracked mechanisms

The very different characteristics of the concrete-GFRP and clay-GFRP interfaces observed in the pull-off tests (Fig. 5) have already been described, and these different responses are also apparent in Fig. 16. The strengthening is less effective for the concrete masonry, due to the inferior interface. Furthermore, the strengthening is less effective for Concrete 2 than Concrete 3, possibly due to imperfections in the masonry-GFRP interface.

Failure of the strengthened masonry

The total shear load carried by the strengthened specimen, v, is conventionally split into two components; the shear carried by an equivalent unreinforced masonry specimen (v_M) and the increase in shear capacity due to strengthening (v_F):

$$v = v_M + v_F \tag{1}$$

In reality, however, the shear carried through the masonry in the strengthened specimen (v_M') is greater than the shear capacity of the unreinforced specimen (v_M). As shown in fig. 17c, the vertical load (n) carried through the masonry is increased by truss action in the GFRP. The increased vertical load confines the masonry and allows it to carry increased shear load during a slip failure in the masonry joints.

The masonry specimens tested were square, hence the diagonal component of the truss in Fig. 17c is at 45° to the vertical, and the increase in compressive load (n_F) due to strengthening is equal to the increase in shear load (v_F). The total load carried by the strengthened specimen is plotted in Fig. 15, which lies outside the failure domain for the masonry. The proportion of the total shear load carried by the masonry (v_M') lies on the failure limit, with the same value of compressive load (as shown in Figs. 14 & 15)

If additional GFRP is applied to the masonry the vertical force will increase, until the point is reached on the interaction diagram where failure of the masonry joints changes from slipping to crushing (Fig. 14). Any further increase in the amount of GFRP will not be efficient, and thus there is an upper limit to the useful amount of GFRP that can be applied to masonry.

DESIGN RECOMMENDATIONS

Simple, relevant equations are required for design. However, care must be taken in extending the specific experimental results presented here to the general design case. The loading arrangement used in the present tests was chosen to model that in a real application, but it is unlikely to be identical:

- the shear load (V) was applied as a point load, and the reaction was concentrated at the opposite corner
- the panel was free along its vertical edges

- it was not possible to control the vertical prestress (N) during the test, and this increased with the shear load (V)

- the GFRP was applied before the vertical load, whereas in reality the weight of the building above would be present when the GFRP is applied.

It is particularly important to recognize that both the FRP and the FRP-masonry interface are brittle and that the masonry is only pseudo-ductile under combined shear and compression. This has important implications for design, since ductility is desirable in structures. Perhaps the most obvious requirement for ductility is during an earthquake, when sustained energy dissipation is necessary under cyclic loading, however, ductility is also a fundamental requirement of structural design.

Design is rarely based on the actual equilibrium state within a structure. A simple equilibrium state may be postulated for design purposes (such as the truss analogies for shear in concrete), or other simplifications made (for example, the plane-section assumption of simple beam theory). If an assumed equilibrium state is used, design relies on the *lower-bound* (or safe load) *theorem of plasticity*, which states that the required load can be carried provided *stress redistribution* can occur. Stress redistribution at the ultimate limit state can only occur if the structure is ductile (Stratford & Burgoyne 2001).

A further reason for ensuring a ductile failure mode is the sensitivity of the FRP-masonry interface to imperfections. Imperfections might be due to poor workmanship (such as poor surface preparation, inadequate wetting of the GFRP or the GFRP not being flat), or defects in the bricks. Stress redistribution is required away from an imperfection and consequently ductility is required in the structure.

Masonry is pseudo-ductile under shear-compression loading. This ductile mode of failure should be exploited when FRP strengthening is applied to masonry, as other modes of failure are brittle and thus cannot be used safely in design. FRP strengthening should be designed to ensure that a shear-compression failure occurs within the masonry. The FRP must not fail prematurely, thus it is necessary to examine compatibility of the FRP with the masonry failure mechanism.

Design equations

Serviceability limit-state

At the serviceability limit-state, there should be no de-bonding of the FRP from the masonry. De-bonding of the FRP from the masonry occurs where the shear strength of the interface is exceeded, and will initiate at any concentrations of shear stress (Fig. 10). This strength depends upon the materials used and the

method of application. The shear stress distribution in the interface depends upon the loading arrangement, geometry and relative stiffness of the FRP and masonry.

In the present case, the GFRP first de-bonded from the masonry at a deflection of around 2 mm. This corresponds to a shear strain of 0.17% in the strengthened panel. For similar loading conditions, this may provide a pragmatic serviceability limit, but should be used with caution.

Ultimate limit-state.

At the ultimate limit-state, the FRP should be designed to exploit the pseudo-ductile shear-compression mode of masonry failure, and should not rely on the brittle FRP-masonry interface. The FRP strengthening must be compatible with this mode of masonry failure.

As described above, compatibility of the FRP with cracked masonry is described by a combination of slip and stretching (Fig. 18), and the characteristics of the interface can vary greatly. The interface failure is brittle and irreversible (unlike the friction across a sliding masonry joint). Furthermore, continued load transfer between the masonry and FRP requires a large area of bonded FRP. Real buildings are subjected to distributed loads, and multiple bands of diagonal cracks are likely to form in the masonry (rather than the single diagonal crack observed in the tests due to concentrated load). The regions of de-bonded FRP associated with these cracks will join, and the whole surface will become fully de-bonded. Thus, load transfer between the masonry and the FRP cannot be relied upon in design.

The spread of de-bonded FRP is arrested by anchorages. In the present tests the GFRP was anchored along the top and bottom of the specimens. Fully de-bonded FRP can be used for design purposes.

As in equation (1), the net shear load carried by a strengthened masonry panel is split into the load carried by an equivalent unreinforced specimen (V_M) and the increase in load due to the FRP (V_F) (Eurocode 6, 1996):

$$V = V_M + V_F \tag{2}$$

V_M has been defined for tests on unreinforced masonry, for example in Eurocode 6 (1996). However, Triantafillou (1998) notes that the strength of the masonry may be reduced if it is damaged prior to strengthening.

The load carried by the FRP (V_F') increases with deflection (δ). The horizontal stiffness (V_F'/δ) of the de-bonded FRP mechanism is modeled by the simple truss mechanism shown in Fig. 20, it is assumed that the de-bonded FRP is linear-elastic, of thickness t_f, with stiffness E_{F_b} parallel to the tensile diagonal (note that FRP is

anisotropic). As the FRP is a sheet and not a truss member, an effective width (w) is used to describe the FRP that is active in carrying tension. The de-bonded length of reinforcement is denoted ℓ.

$$\frac{V_F{'}}{\delta} = \frac{w t_F E_{F\theta}}{\ell}$$

(3)

The effective width, w, describes the variation in strain in the FRP along the crack. w includes the effects of specimen geometry, the position of anchorages and the fixity of the panel edges.

The FRP must not fail before the masonry and so must have a deflection capacity greater than δ_1, the deflection-capacity of the unreinforced masonry. (Figure 12 shows that δ_1 was 14 mm for clay or 12 mm for concrete in the present tests). Assuming the truss mechanism shown in Fig. 20, the strain in the FRP for a deflection of δ_1 is:

$$\varepsilon_1 = \frac{\delta_1}{\ell \cos\theta}$$

(4)

The strain capacity of the FRP must be greater than ε_1 (in the direction of the tensile diagonal).

Furthermore, any fixed anchorage of the FRP to the masonry (in this case, along the top and bottom of the wall) must not fail under a load of

$$V_{F1}{'} = \frac{w t_f E_{f\theta}}{\ell} \delta_1$$

(5)

$V_{F1}{'}$ is the load carried through the FRP at failure of masonry. The FRP also increases the load carried through the masonry ($V_M{'}$), due to confinement by the vertical compression shown in Fig. 20. This additional vertical compression is:

$$N_{F1} = V_F{'}\tan(\theta)$$

(6)

The additional shear load carried by the masonry can be found using the interaction diagrams for failure of the masonry, as in Fig. 15.

Design options

Equations (4) & (5) allow failure of the FRP strengthening to be predicted. There initially appears to be very little flexibility for the designer in these equations: the ultimate-tensile –strain of the reinforcemenet and the effectiveness of the anchorages can only be adjusted within narrow limits. However, another option is to change

the de-bonded length (ℓ) of the reinforcement. Reducing ℓ increases the stiffness of the de-bonded FRP (equation (3)), but reduces its deformation-capacity (equation (4)).

The de-bonded length of FRP is determined by the anchorage arrangements. In the tests described above, the FRP was anchored along the top and bottom edges of the panel. If the FRP was anchored in a similar manner in buildings (i.e.: at floor and ceiling level), the de-bonded length would be considerably longer, and the strengthening would not be so effective.

The de-bonded length can be reduced by introducing intermediate anchorages. An intermediate anchorage can be effected by chasing out a horizontal joint in the masonry, and the sheet reinforcement trapped in this joint by bonding in an FRP bar. This anchorage arrangement has successfully been used to fix sheet FRP to concrete beams (Khalifa et al. 1999), and is similar to the near-surface mounted bar concept (Fig. 1a), although it requires fewer joints to be chased out.

CONCLUSIONS

Sheet FRP can be easily applied as masonry strengthening. The present research (with fibers orientated parallel to the masonry joints) has shown that sheet FRP strengthening increases the load-capacity of masonry subjected to in-plane shear loading.

Care is necessary in applying the present test results in design. The strengthened masonry includes brittle components (the FRP and the masonry-FRP interface), failure of the test specimens is characterized by brittle failure across the interface. If premature failure of the FRP strengthening is avoided, a ductile failure occurs within the masonry joints. The strengthening should be designed to exploit this masonry joint ductility. Failure in the masonry can be ensured by controlling the de-bonded length of the FRP using intermediate anchorages.

An interesting observation is that if ultimate-limit-state design is based on de-bonded FRP, the adhesive used to apply the FRP to the masonry need not be strong. The adhesive should be selected for its strain-capacity rather than its strength. This may allow the use of an adhesive that does not burn and produce toxic fumes.

The present work is not exhaustive, and further development work is planned. For example, cyclic loading must be investigated, the suggested design equations checked and calibrated, and anchorage arrangements investigated.

APPENDIX. NOTATION

b = breadth of panel;

E_{F_s} = stiffness of FRP in direction of the tensile diagonal;

h = height of panel;

H = horizontal load carried by the reaction beam;

ℓ = de-bonded length of strengthening;

$n\,/\,N$ = (non-dimensional) vertical load applied to a specimen;

n_F = non-dimensional increase in compressive load through masonry due to GFRP;

N_{F1} = additional compressive load carried through masonry due to GFRP;

P = total applied horizontal load ($P=V+H$);

t_F = thickness of FRP;

t_M = thickness of masonry;

$v\,/\,V$ = (non-dimensional) net shear load carried by a strengthened masonry panel;

$v_F\,/\,V_F$ = (non-dimensional) increase in shear load due to GFRP strengthening;

$v_F{'}\,/\,V_F{'}$ = (non-dimensional) shear load carried through the GFRP;

$v_M\,/\,V_M$ = (non-dimensional) shear load carried by the equivalent unreinforced masonry;

$v_M{'}\,/\,V_M{'}$ = (non-dimensional) shear load carried through the masonry;

w = the "effective width" over which strengthening carries load;

δ = horizontal deflection of panel (measured at the level of the applied load, but on opposite side of panel);

δ_1 = horizontal deflection-capacity of the unreinforced masonry ;

ε = Strain measured in the GFRP;

ε_1 = strain-capacity of the GFRP in the direction of the tensile diagonal (at angle θ);

$\bar{\sigma}$ = compressive strength of the masonry; and

θ   =   angle of the tensile diagonal to the horizontal.

REFERENCES

Al-Saidy, A., Ehsani, M. R., and Saadatmanesh, H. (1996). *"Strengthening of URM walls for direct shear"* , in El-Badry M. M., *Advanced composite materials in bridges and structures – Second international conference*, The Canadian Society for Civil Engineering, 605-612.

Arduini, M., and Nanni, A. (1997) "Behavior of precracked RC beams strengthened with carbon FRP sheets", *Journal of Composites for Construction*, Vol. 1, No. 2, pp. 63-70.

Barsotti, R., and Ligarò, S. (1998). "Non-linear analysis of un-reinforced masonry buildings under horizontal loads"*, Computer Methods in structural masonry – 4*, Eds. Pande, Middleton and Kralj, E & FN Spon, New York, 277-284.

Ehsani, M.R, (1995). *"Strengthening of earthquake-damaged buildings"*, in *Non-metallic (FRP) reinforcement for concrete structures* – proceedings of the second international RILEM Symposium, Rilem Proceedings 29, E & FN Spon, 680-687.

Eurocode 6 (1996). "Eurocode 6: Design of masonry structures". European Committee for Standardization.

Fam A.Z., Rizkalla S.H., and Tadros G. (1997) "Behavior of CFRP for Prestressing and Shear Reinforcements of Concrete Highway Bridges", *ACI Structural Journal*,V.94, No.1, 77-86.

Hamid, A., Larralde, J., and Salama, A., (1993). "Properties of hollow concrete masonry reinforced with fiberglass composite", in *Fiber-reinforced-plastic reinforcement for concrete structures* – International Symposium, American Concrete Institute, SP 138-26, 465-474.

Khalifa, A., Alkhrdaji, T., Nanni, T., and Lansburg, S. (1999). "Anchorage of Surface Mounted FRP Reinforcement," *Concrete International: Design and Construction*, 21(10), 49-54.

Kolsch, H., (1998). "Carbon fiber cement matrix (CFCM) overlay system for masonry strengthening", *Journal of composites for construction*, 2(2), 105-109.

Luciano, R., and Sacco, E. (1998) "Damage of masonry panels reinforced by FRP sheets", *International Journal of Solids and Structures* 35(15), 1723-1741

Marshall, O.S., Sweeney, S.C., and Trovillion, J.C., (1999). *"Seismic rehabilitation of unreinforced masonry walls", SP 188-26*, 287-295.

Schwegler, G., (1994). "Verstäken von mauerwerk mit faserverbundwerkstoffen in seismisch gefährdeten

zonen*", Bericht Nr. 229*, EMPA, Dübendorf.

Stratford T.J., and Burgoyne C.J. (2001). "Shear analysis of concrete with brittle reinforcement". In *FRPRCS-5*, Cambridge, UK, 939-948

Tinazzi, D., Modena, C., and Nanni, A., (2000). *"*Strengthening of masonry assemblages with FRP rods and laminates", In *International Meeting on Composite Materials, PLAST 2000, Advancing with Composites*, Ed. I. Crivelli-Visconti, Milan, Italy, 411-418.

Triantafillou, T.C., (1998). *"*Strengthening of masonry structures using epoxy-bonded FRP laminates*"*, *ASCE journal of composites for construction*, **2**(2), 96-104.

Tumialan, G., Huang, P-C., Nanni, A., and Silva P., (2001). "Strengthening of masonry walls by FRP structural repointing". In *FRPRCS-5*, Cambridge, UK, 1033-1042

(a) Near-surface mounted
FRP bars

(b) Strip FRP, arranged
as a truss

(c) Sheet FRP
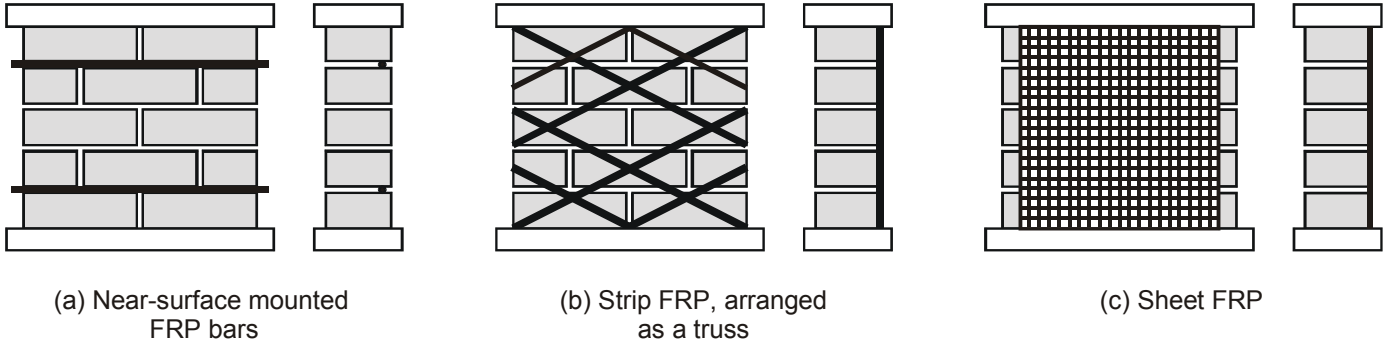
Figure 1 - Alternative approaches to strengthening masonry structures using FRP

Weight of
building above

In-plane
shear load

Brick wall

Filler
layer

1.2m

1.2m

Sheet FRP
reinforcement
in epoxy adhesive
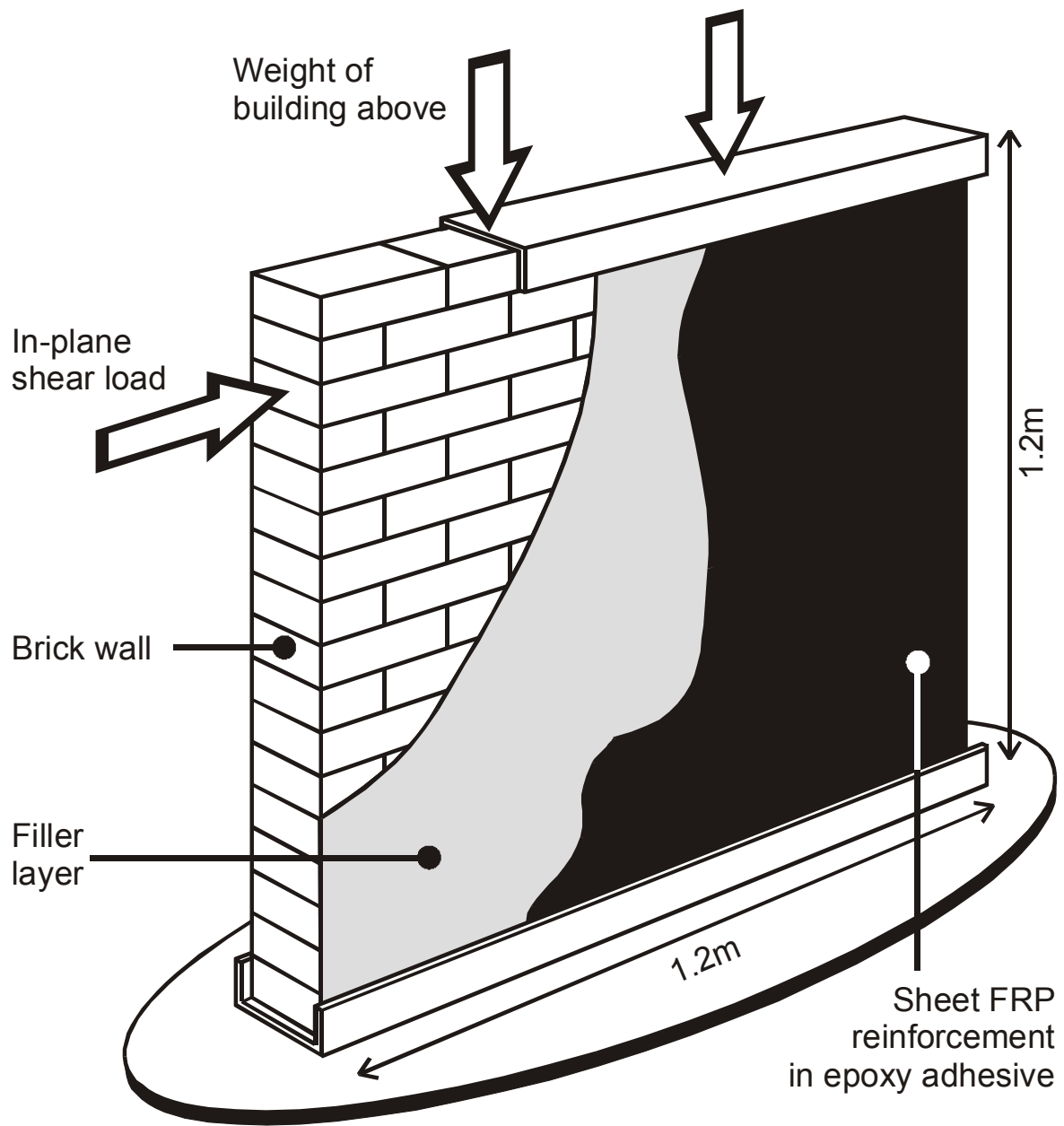
Figure 2 - In-plane shear strengthening using sheet GFRP - schematic arrangement.

Figure 3 - The testing frame.

N/2   0.6   N/2

Threaded bars

H

Reaction beam

P

Cap beam

PTFE bearing

δ

0.45   ε

1.0

0.5

1.0

1.2
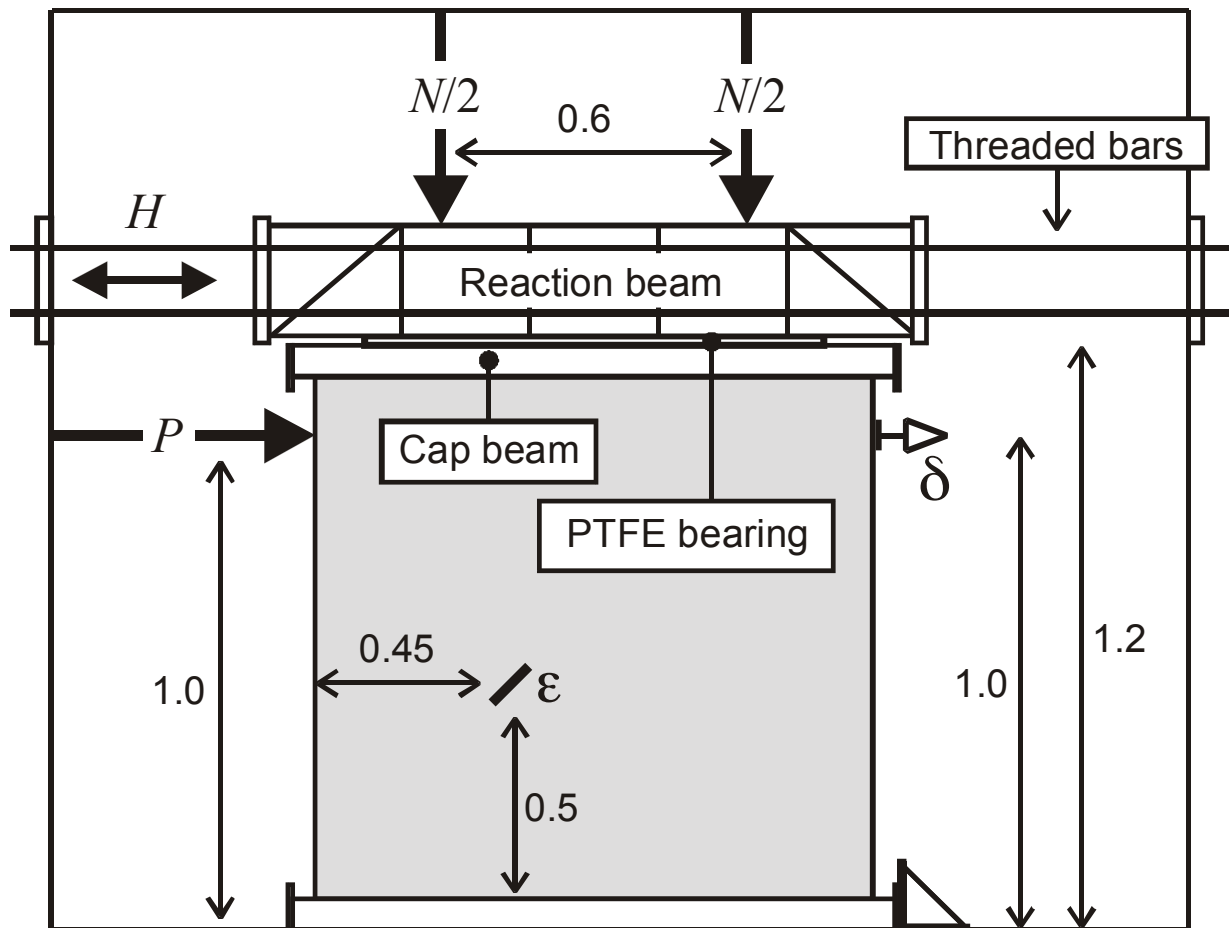
Figure 4 - Test apparatus arrangement.

a) Clay   b) Concrete

Figure 5 - Interface failure in the small-scale pull-off specimens.

Figure 6 - Crack pattern in the unreinforced clay panel (clay 1).

Figure 7 - Crack pattern in the unreinforced concrete panel (concrete 1).
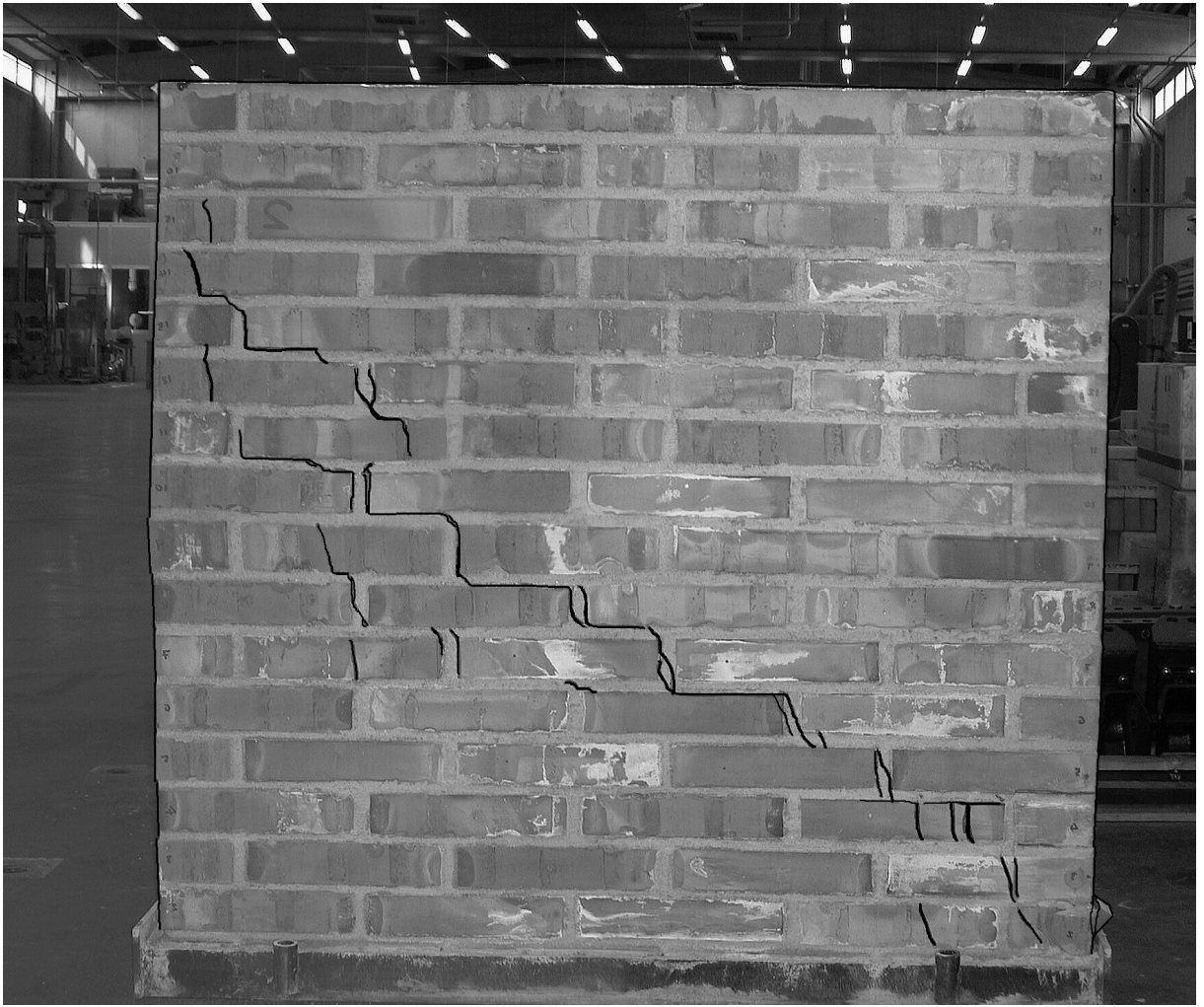
Figure 8 - Crack pattern in a strengthened clay panel (clay 2).
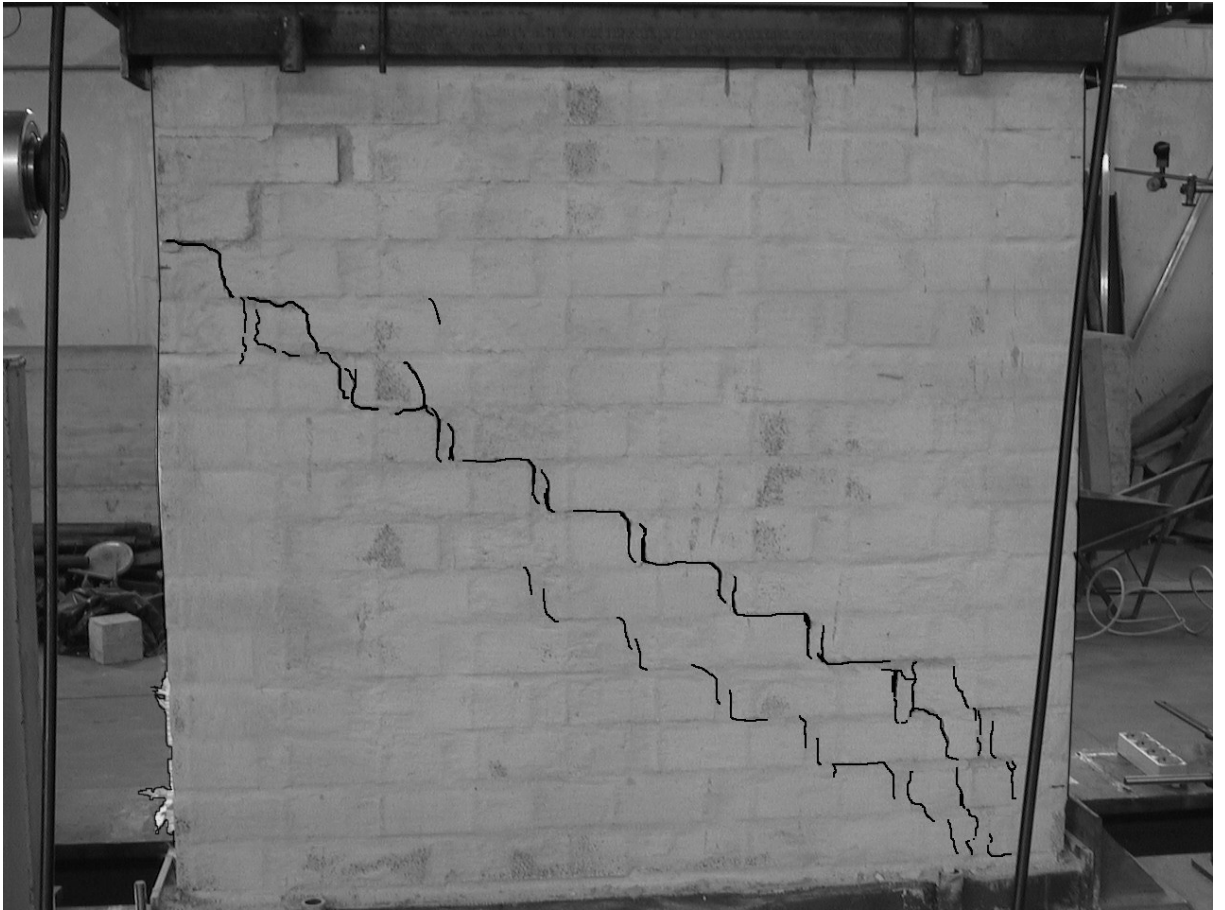
Figure 9 - Crack pattern in a strengthened concrete panel (concrete 3).
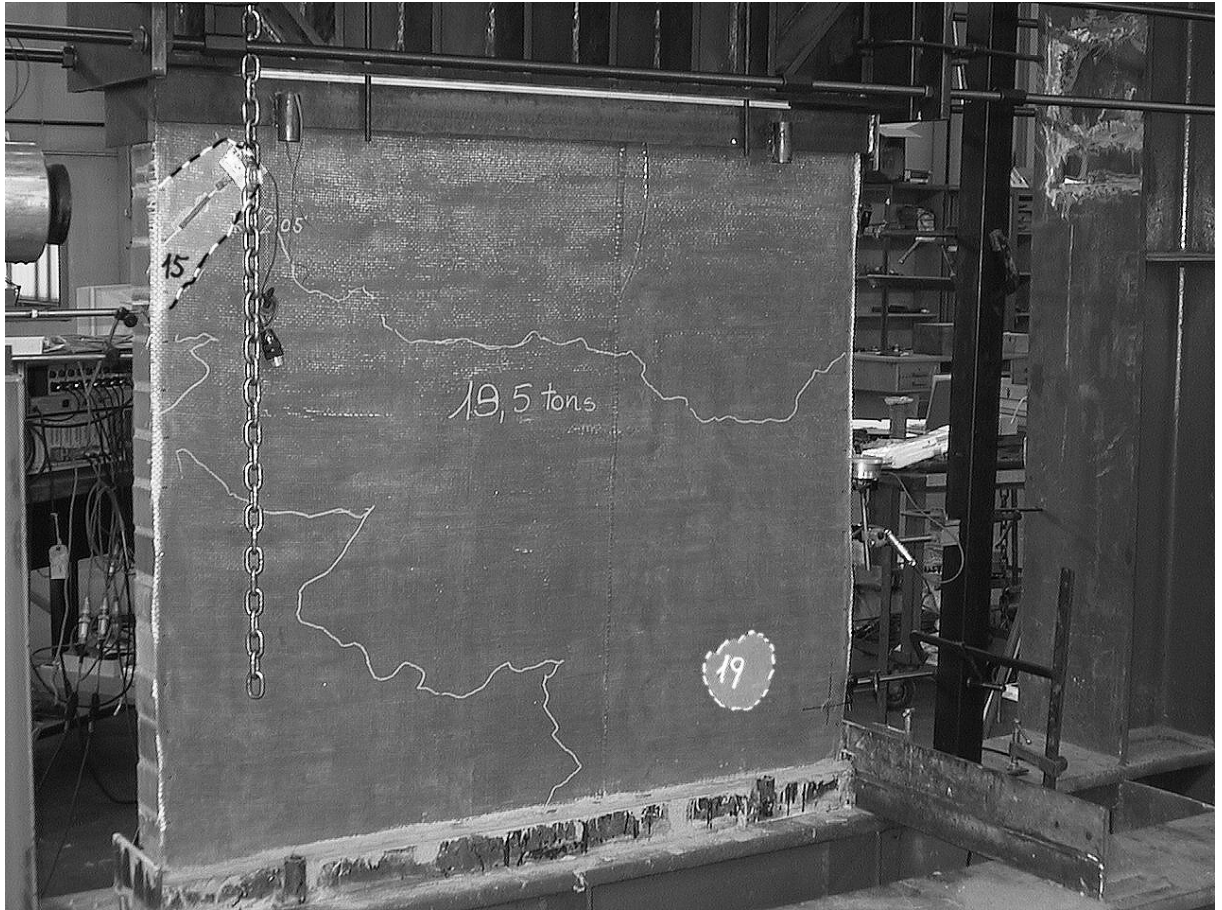
Figure 10 - Extent of de-bonding of the strengthening for clay 2. (Post-processed for clarity).

Figure 11 - Failure of the GFRP-masonry interface in a clay panel.
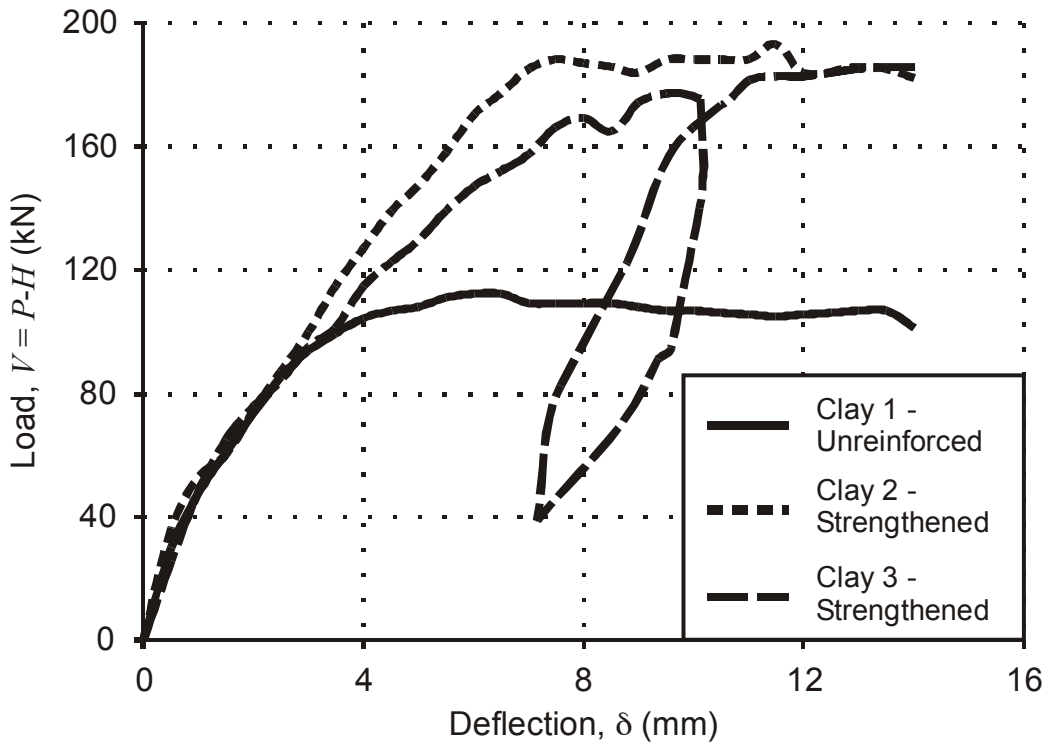
(a) Clay specimens
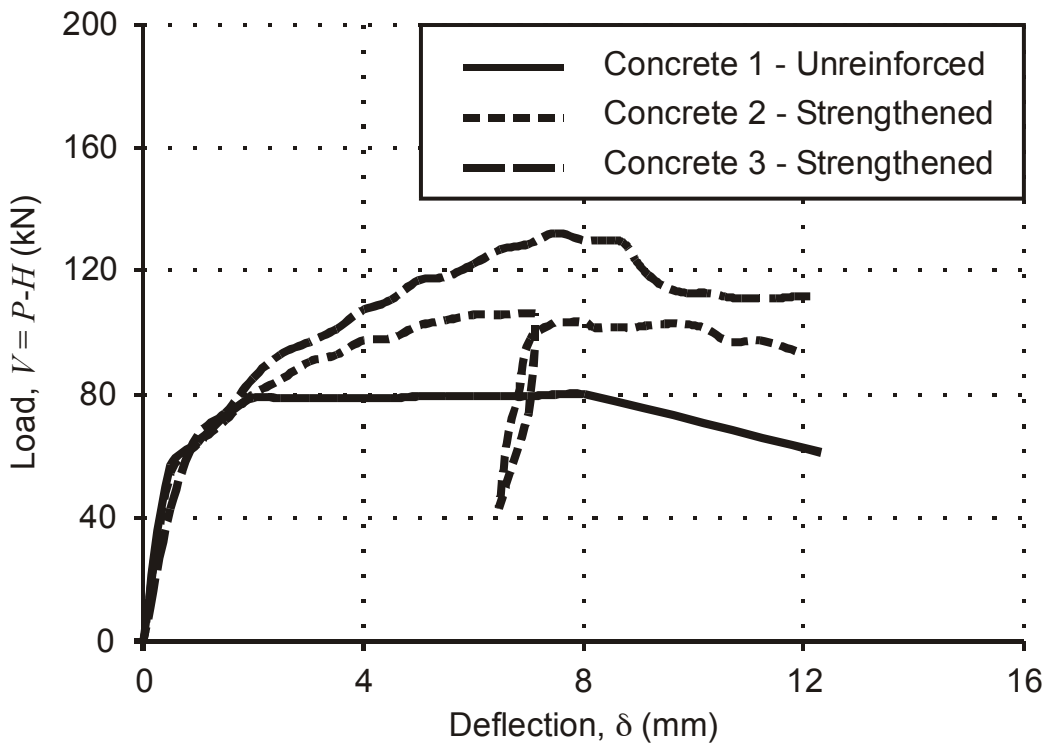
(b) Concrete specimens

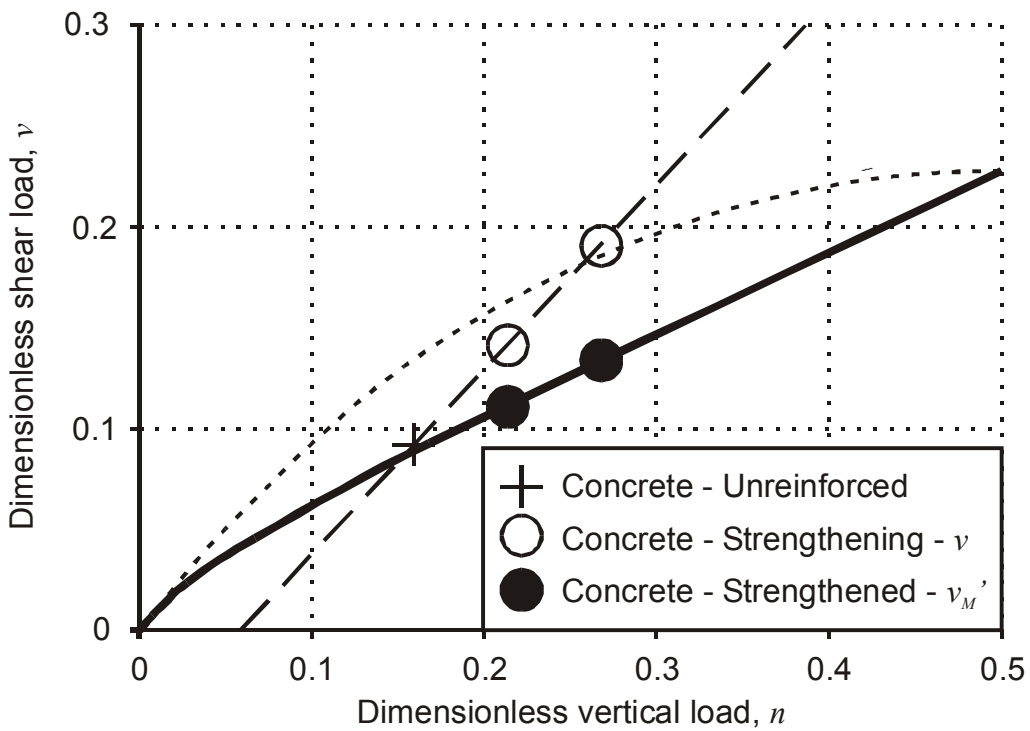Figure 12 - Load-deflection responses.
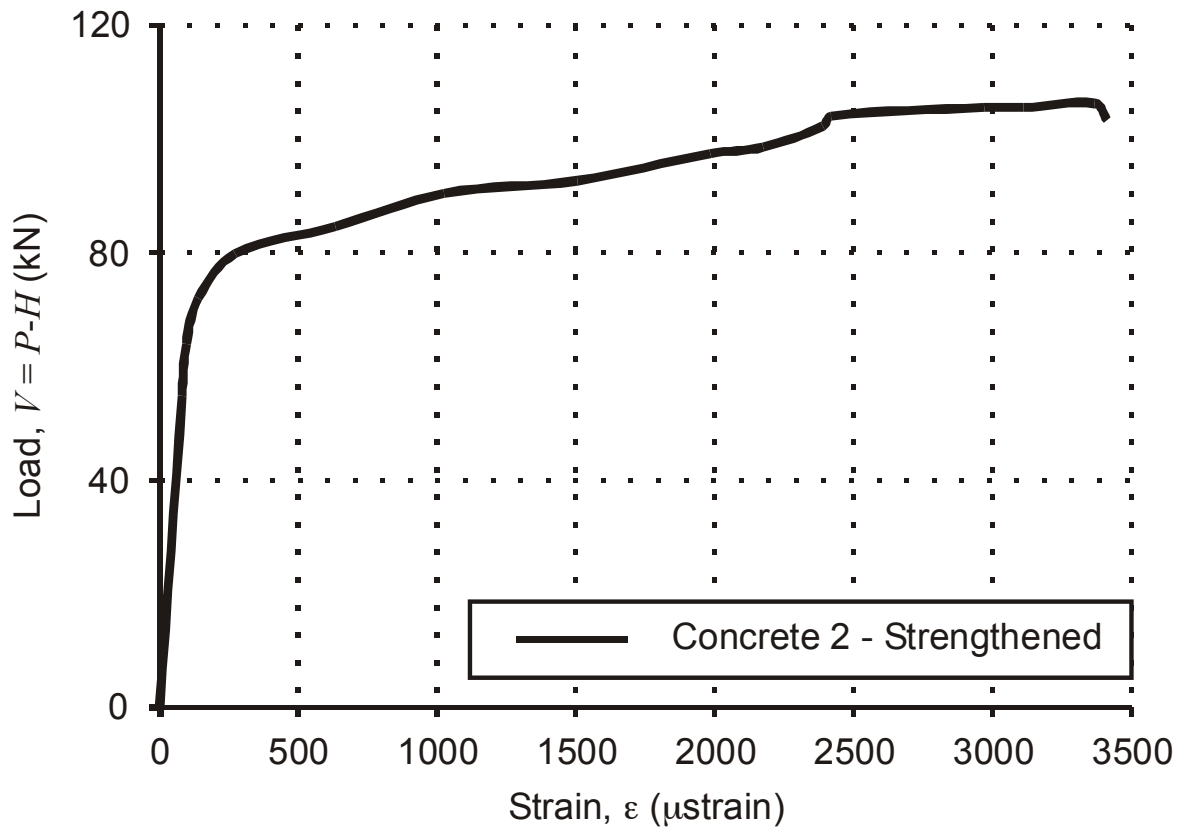
Figure 13 - Load-strain response.
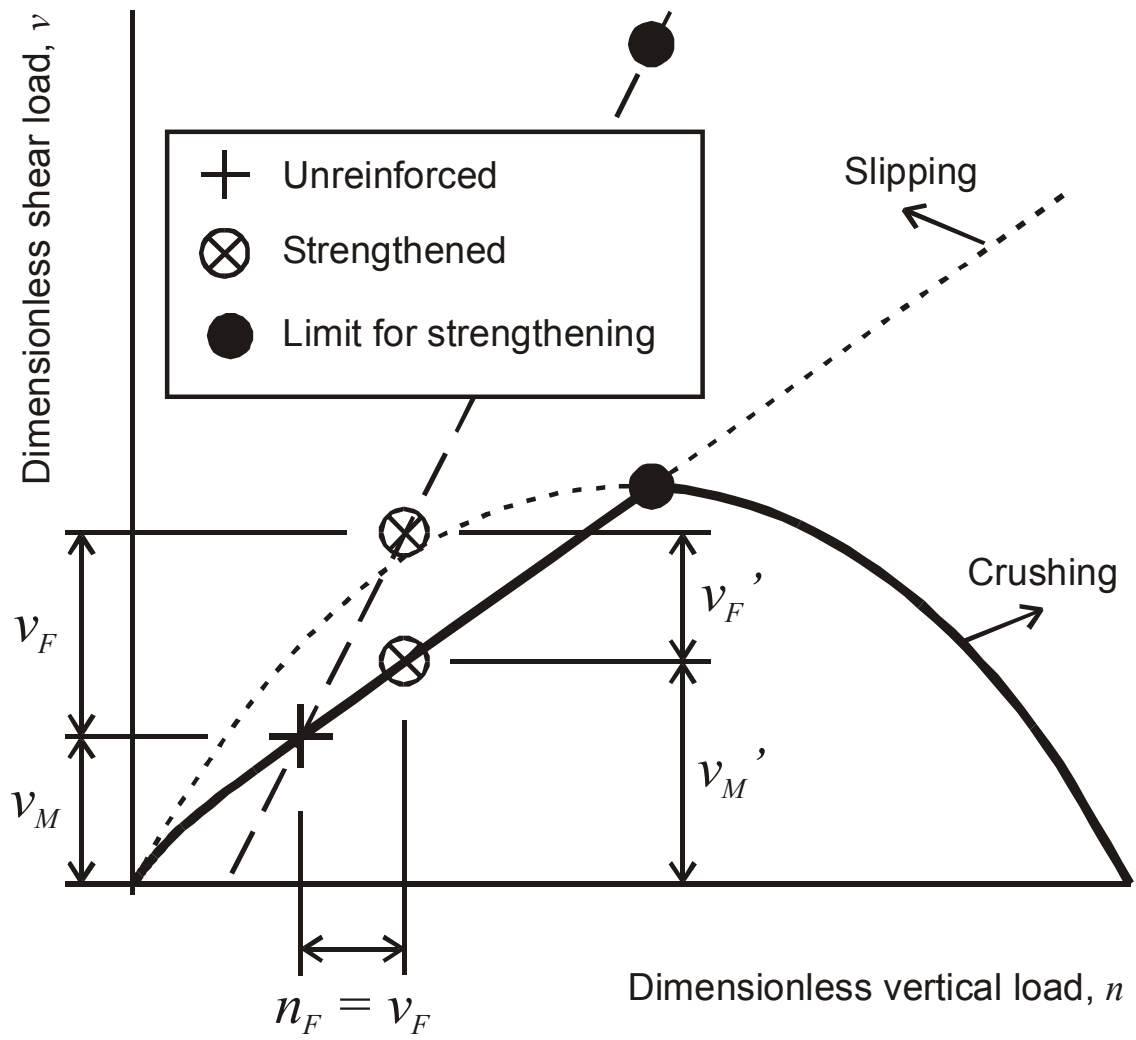
Figure 14 - Interaction diagram for masonry failure.
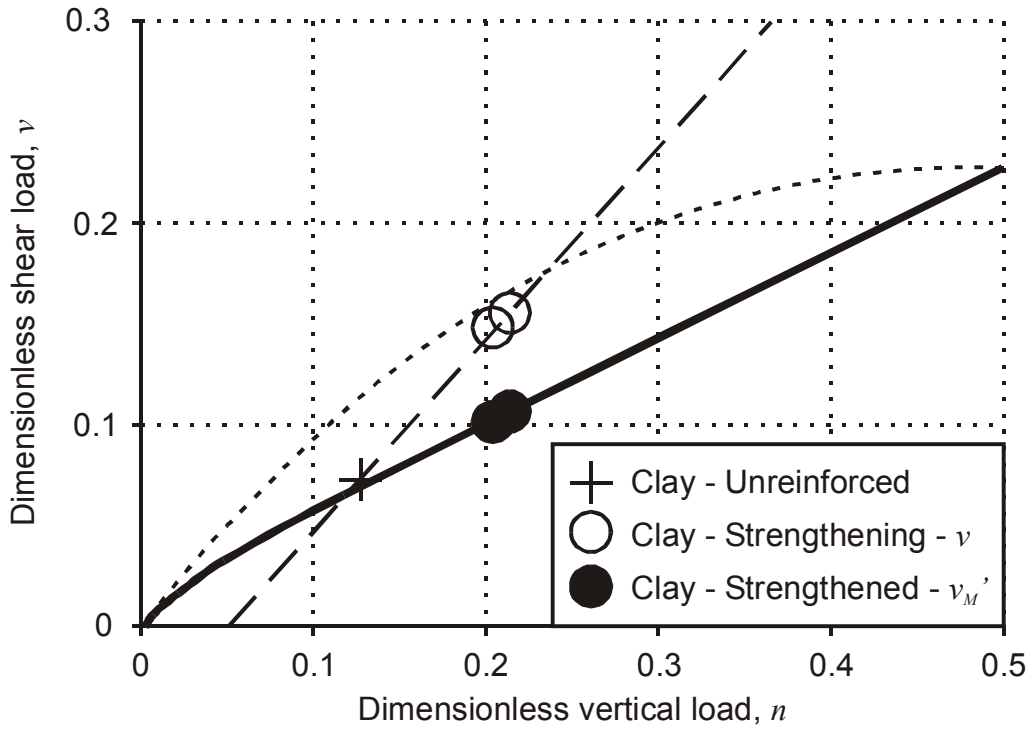
(a) Clay specimens

(b) Concrete specimens

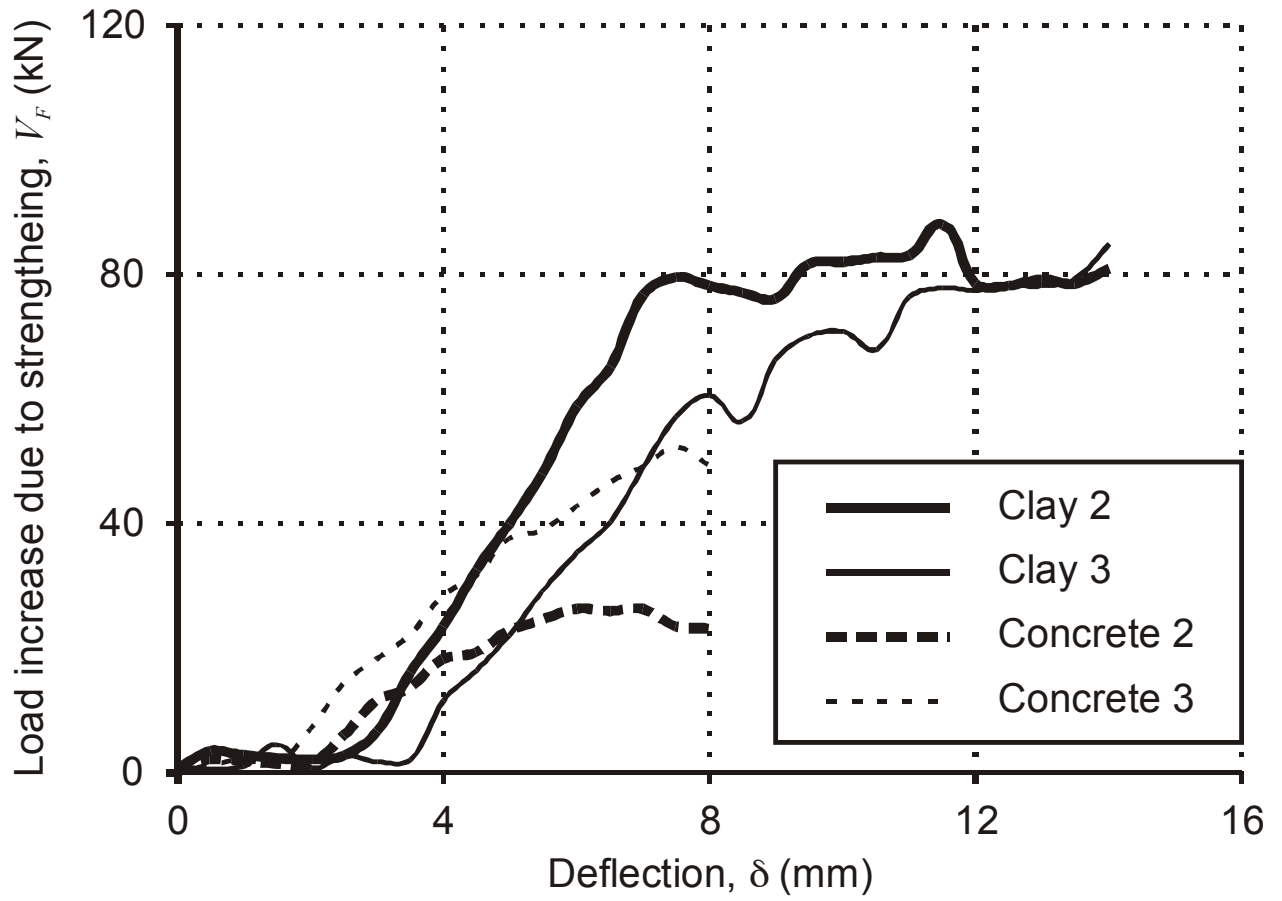Figure 15 - Interaction diagrams for failure of the clay and concrete specimens.

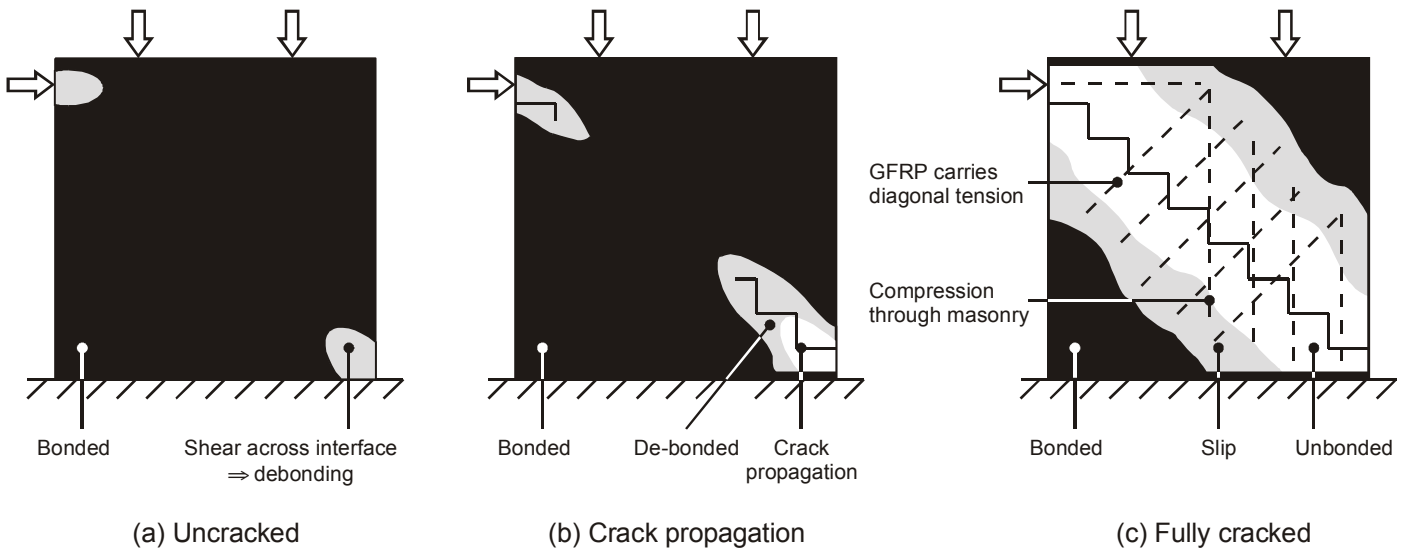Figure 16 - Increase in load with deflection due to strengthening.

Figure 17 - The three mechanisms by which the strengthening carries load.
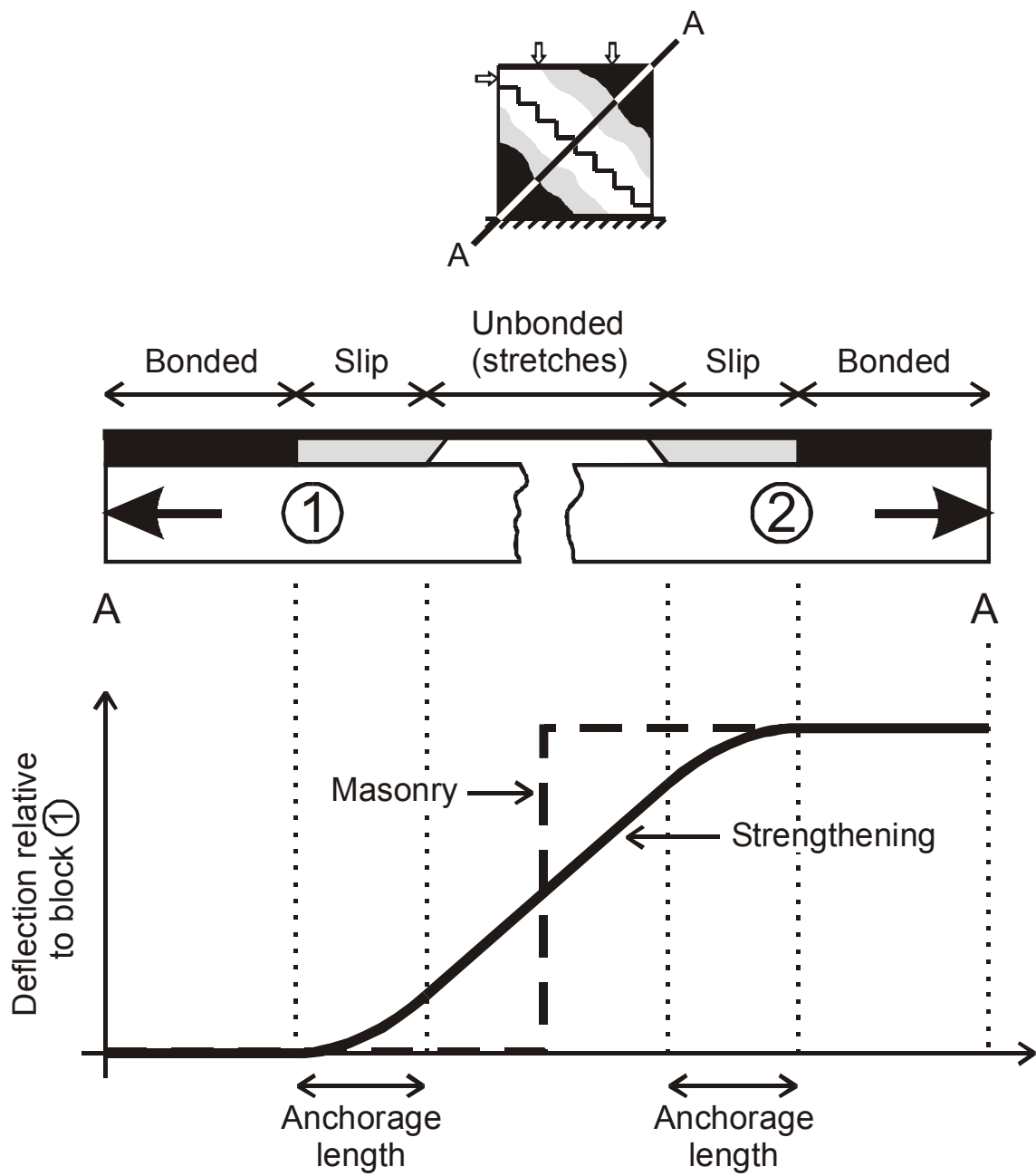
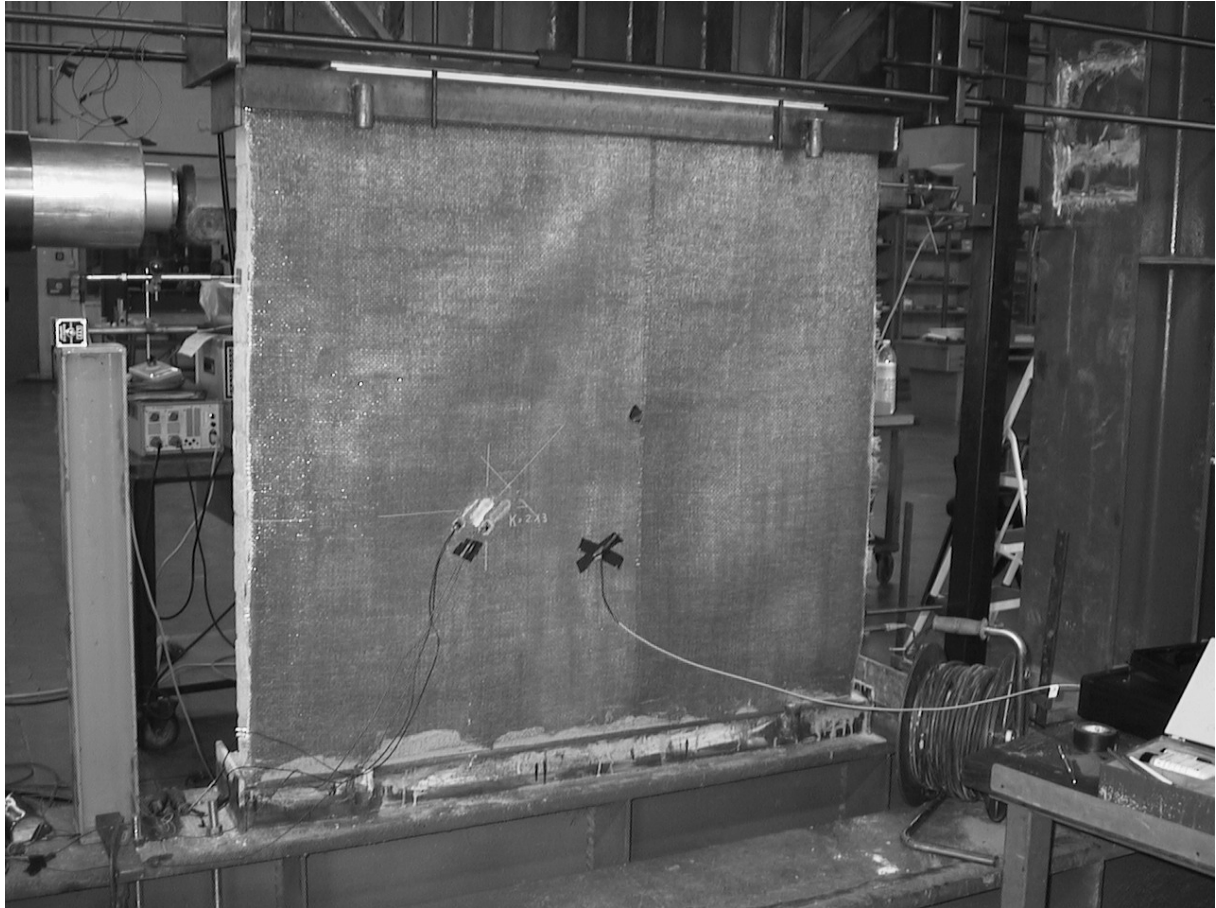Figure 18 - Compatibility of the partially de-bonded strengthening.

Figure 19 - Diagonal banding of the strengthening, due to the formation of shear waves (Specimen concrete 3).
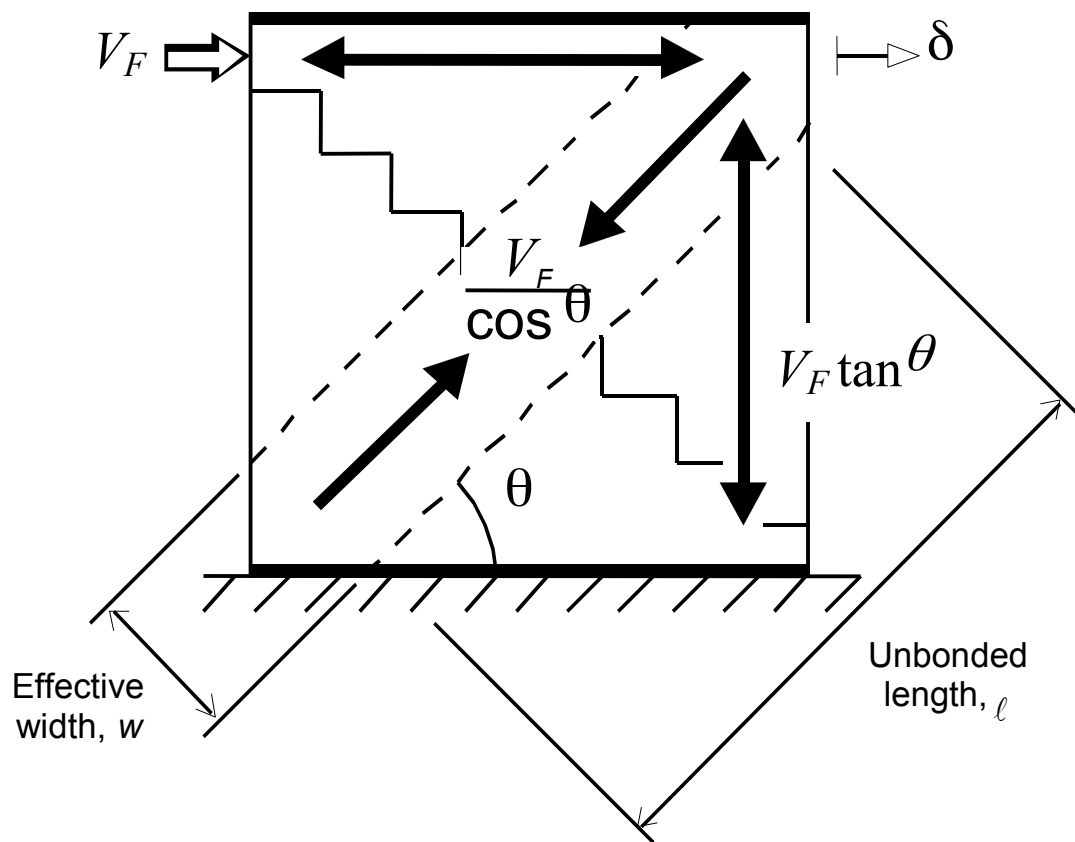
Figure 20 - Truss mechanism for carrying load through the de-bonded strengthening.

Table 1 - Details of the masonry specimens.

Specimen	Material	GFRP strengthening
(1)	(2)	(3)
Clay 1	Clay	Un-reinforced
Clay 2	Clay	Strengthened
Clay 3	Clay	Strengthened
Concrete 1	Concrete	Un-reinforced
Concrete 2	Concrete	Strengthened
Concrete 3	Concrete	Strengthened

Table 2 - Results of the material characterization tests.

Item (1)	Property (2)	Clay wall (3)	Concrete wall (4)	Method (5)
Brick	Compressive strength	62 MPa	36 MPa	Compressive test on 60mm cube
	Tensile strength	8.9 MPa	5.9 MPa	Flexural rupture of 180×60×60mm specimen
	Young's modulus	15.8 GPa	30.2 GPa	UNI 9724 /RILEM CPC 8
	Poisson's ratio	0.13	0.20	
Mortar (within masonry joint)	Compressive strength	> 11 MPa	5.5 MPa	Compressive tests on small wall specimens
	Young's modulus	0.32 GPa	0.06 GPa	
GFRP composite	Nominal thickness	0.15mm		ASTM D 3039/3039M 95a
	Tensile strength (0° direction)	147.9 N/mm		
	Stiffness (0° direction)	11000 N/mm		